AIR ABSORPTION FILTERING METHOD BASED ON APPROXIMATE GREEN'S FUNCTION FOR STOKES' EQUATION

Brian Hamilton

Acoustics & Audio Group
University of Edinburgh
Edinburgh, UK
bhamilton.ac@gmail.com

ABSTRACT

Air absorption effects lead to significant attenuation in high frequencies over long distances and this is critical to model in wide-band virtual acoustic simulations. Air absorption is commonly modelled using filter banks applied to an impulse response or to individual impulse events (rays or image sources) arriving at a receiver. Such filter banks require non-trivial fitting to air absorption attenuation curves, as a function of time or distance, in the case of IIR approximations, or may suffer from overlap-add artefacts in the case of FIR approximations. In this study, a filter method is presented which avoids the aforementioned issues. The proposed approach relies on a time-varying diffusion kernel that is found in an approximate Green's function solution to Stokes' equation in free space. This kernel acts as a low-pass filter that is parametrised by physical constants, and can be applied to an impulse response using time-varying convolution. Numerical examples are presented demonstrating the utility of this approach for adding air absorption effects to room impulse responses simulated using geometrical acoustics or wave-based methods.

1. INTRODUCTION

Air absorption leads to significant dissipation in high frequencies over long distances and it is crucial to include these effects in wide-band virtual acoustic simulations for auralization [1], artificial reverberation [2], and auditory research [3]. In wave-based simulation methods, air absorption may be simulated directly from lossy wave models [4, 5, 6], but computational complexity must naturally increase over lossless models – e.g., at least a 50% increase in memory in time-domain methods [7] – and computational costs are already quite high when the aim is to accurately simulate high frequencies. In geometrical acoustics methods – which are more commonly used for virtual acoustics [8] – and in delay networks for artificial reverberation [9, 10, 11], air absorption is typically modelled using digital filters. However, any filter approach is complicated by the fact that air absorption is a distance-dependent effect that does not trivially translate to simple filter structures. When separate frequency-band geometrical simulations are run, one can apply distance-based energy-attenuation to image sources or rays, and subsequently recombine band-specific simulation outputs with appropriate filter banks [12, 13, 8]. Alternatively, one can fit low-order IIR low-pass filters to air absorption data and apply them to individual rays or image sources [14, 15] that make up an impulse response.

This work was funded in part by grant ERC-StG-2011-279068-NESS.

Rather than apply air attenuation to each image source or ray, one can also simulate lossless sound propagation in air and post-process resulting impulse responses with time-varying low-pass IIR filters, using non-linear optimisations against air absorption curves at each time-sample to obtain filter coefficients [16]. Similarly, window-method-designed FIR filters can be used in an overlap-add time-frequency modification framework [17, 18] and this has the advantage that air absorption attenuation curves may be sampled directly in the frequency-domain. The overlap-add FIR approach is straightforward, but inherent are the usual time-frequency resolution trade-offs (high frequency resolution requires long time windows) and possible phase incoherences at frame overlaps [19]. Processing of individual image sources or rays would also be possible with window-method FIR filters [20, 21] but – for computational efficiency reasons – is less common than the use of low-order IIR filters [15].

In this paper, an alternative approach is proposed which sidesteps all of the aforementioned issues. From a high level, this method is another time-varying filter method applied to a room impulse response simulation without air absorption. However, the proposed method does not suffer from the usual time-frequency artefacts and does not require IIR filter fitting. It is expressed as a convolution with a time-varying smoothing kernel derived from a physical model for classical air absorption, with an efficient discrete implementation. Numerical experiments are presented to show the effectiveness of the proposed method in the context of geometrical and wave-based simulations.

2. BACKGROUND

2.1. Air absorption model

The standard model of air attenuation due to atmospheric effects can be described by the frequency-dependent attenuation factor coefficient $\alpha(\omega)$, which appears in a distance-based exponential damping applied to an otherwise lossless plane wave; i.e.:

$$p(x,t) = e^{-\alpha(\omega)x} e^{i(kx-\omega t)} \Rightarrow |p(x,t)| = e^{-\alpha(\omega)x} |p(0,t)|\,, \tag{1}$$

with real-valued angular frequency ω and wavenumber k, and wave-quantity p (e.g., pressure). According to the literature [22], $\alpha(\omega)$ can be expressed as:

$$\alpha(\omega) = \underbrace{\frac{\gamma\omega^2}{2c}}_{\alpha_{\text{cl}}} + \sum_{\nu} \underbrace{\frac{(\alpha_\nu \lambda)_m}{\pi c} \frac{\omega^2 \tau_\nu}{1+(\omega\tau_\nu)^2}}_{\alpha_\nu}\,, \tag{2}$$

where c is the sound speed (assumed constant), γ is a time constant related to viscothermal effects, $(\alpha_\nu\lambda)_m$ represents the maximum absorption per wavelength associated with the ν-type relaxation

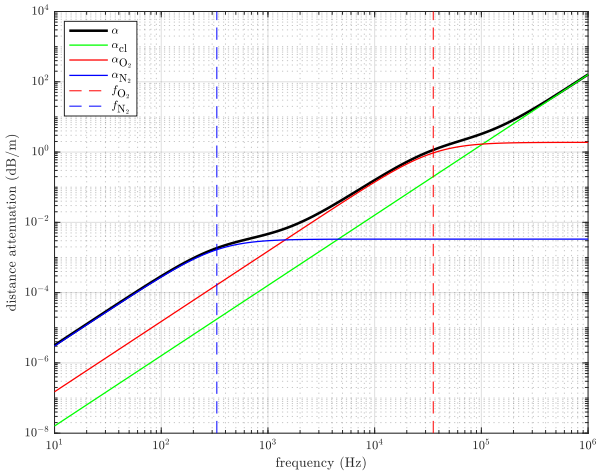

Figure 1: Distance attenuation in dB/m as a function of frequency, for air conditions of 20°C and 50% relative humidity.

process, and τ_ν is the associated relaxation time. Conventionally we consider two relaxation processes: one from oxygen molecules and one from nitrogen molecules ($\nu \in \{\mathrm{O}_2, \mathrm{N}_2\}$). The associated phase speed is frequency-dependent in theory, but typically varies from c by less than 0.04% across audible frequencies [22]. The constants in (2) depend on temperature and humidity, for which the full details may be found in the literature (e.g., [23, 24]).

The air absorption model in (2) has three parts: the first term, α_{cl}, represents classical power-law absorption ($\alpha_{\mathrm{cl}} \propto \omega^2$), which comes from viscothermal effects [22] and which been included in wave-based room simulation models [5, 7, 25]. Additionally there are two relaxation effects $\alpha_\nu \in \{\alpha_{\mathrm{O}_2}, \alpha_{\mathrm{N}_2}\}$. These relaxation effects have the following behaviours:

$$\alpha_\nu(\omega) \approx \omega^2 \frac{(\alpha_\nu \lambda)_m \tau_\nu}{\pi c}, \quad \omega \ll 1/\tau_\nu \tag{3a}$$

$$\alpha_\nu(\omega) \approx \frac{(\alpha_\nu \lambda)_m}{\pi c \tau_\nu}, \quad \omega \gg 1/\tau_\nu \tag{3b}$$

In other words, below the associated relaxation frequency, $f_\nu = (2\pi\tau_\nu)^{-1}$, a relaxation effect tends to contribute a power-law absorption, and a constant absorption above the relaxation frequency. A graphical representation of these three effects is shown in Fig. 1 for typical indoor air conditions.

It is worth pointing out that, as can be seen in Fig. 1, air attenuation can vary by large amounts within octave bands. For example, one finds a variation of 39dB/km and 143dB/km across upper and lower edge-frequencies of the 4kHz and 8kHz octave bands, respectively for these air conditions. Thus, it is problematic to only use one averaged air attenuation coefficient per octave band. Not surprisingly, this common practice has been shown to lead to incorrect predictions [26]. Using third-octave band data would lead to improvements, but errors are still bound to increase with increasing frequency bands and could potentially exceed masking thresholds [27].

Fig. 1 also shows that, at least for this choice of indoor conditions, absorption from oxygen molecules is the dominant effect in high frequencies (below the audible limit), and that is mostly a power-law effect. Looking towards lower frequencies, the behaviour deviates from a power law near the relaxation frequency of nitrogen, but this is already at a point where the effect of air absorption starts to be negligible in the context of room acoustics (e.g., 1.5dB attenuation per km at f_{N_2}). It is therefore reasonable to model only the power-law absorption from oxygen, as in [7]. As such, for the proposed approach we rely on the following assumption for audible frequencies:

$$\alpha(\omega) \approx \tilde{\alpha}_{\mathrm{O}_2}(\omega), \quad \tilde{\alpha}_{\mathrm{O}_2}(\omega) = \omega^2 \frac{(\alpha_{\mathrm{O}_2}\lambda)_m \tau_{\mathrm{O}_2}}{\pi c} \tag{4}$$

2.2. Stokes' equation

The proposed method is primarily based on Stokes' equation [28], which can be written in the inhomogeneous form:

$$\frac{1}{c^2}\partial_t^2 g - \nabla^2 g - \gamma' \partial_t \nabla^2 g = \delta(t)\delta(\mathbf{x}) \tag{5}$$

Here, $g = g(t, \mathbf{x})$ is the Green's function for (5), t is time, $\mathbf{x}$ is a 3-D spatial coordinate, ∂_t is a temporal partial derivative, ∇^2 is the 3-D Laplacian operator, $\delta(t)$ is the Dirac delta in time, and $\delta(\mathbf{x})$ is a 3-D Dirac delta in space. The constant γ' is a time-constant and is typically on the order of one nanosecond (for indoor air). Without loss of generality, the source term is centered at the origin so that any receiver will be at distance $R = \|\mathbf{x}\|$. In the case of $\gamma' = 0$, Eq. (5) reduces to the wave equation in inhomogeneous form. In Stokes' original formulation γ' only included viscous effects [28], but one can lump in thermal effects as well [22].

It is straightforward to check that the dispersion relation for the homogeneous form of (5) (with right-hand side equal to zero) is:

$$\hat{k} = \frac{\omega}{c\sqrt{1 - i\gamma'\omega}} \tag{6}$$

where $\hat{k}$ is a complex wavenumber. When $\omega\gamma' \ll 1$, one has the approximation:

$$\hat{k} \approx \frac{\omega}{c} + i\frac{\gamma'\omega^2}{2c} \tag{7}$$

While the real part of the above is clearly the dispersion relation of the wave equation, the imaginary part describes a distance-based attenuation coefficient. Normally then one would set $\gamma' = \gamma$ and this would reproduce the classical air absorption coefficient, α_{cl} (with, e.g., $\gamma = 3.2 \times 10^{-10}$ s for the air conditions in Fig. 1). However, under the assumption (4) we instead take the following value:

$$\gamma' = \frac{2}{\pi}\tau_{\mathrm{O}_2}(\alpha_{\mathrm{O}_2}\lambda)_m = \frac{(\alpha_{\mathrm{O}_2}\lambda)_m}{\pi^2 f_{\mathrm{O}_2}} \tag{8}$$

As such, we will have $\Im\{\hat{k}(\omega)\} \approx \tilde{\alpha}_{\mathrm{O}_2}(\omega)$, linking Stokes' equation to our choice of a simplified model of air absorption (as in [7]). Expressions for $(\alpha_{\mathrm{O}_2}\lambda)_m$ and f_{O_2} are left out for brevity but may be found in [23]. With the air conditions in Fig. 1, one arrives at $\gamma' = 3.0 \times 10^{-9}$ s.

3. APPROXIMATE GREEN'S FUNCTION METHOD

3.1. Approximate Green's function

Returning to the inhomogeneous form of Stokes' equation, in the case of $\gamma' = 0$, Eq. (5) has a well-known Green's function solution [29] $g = g_\Box$, where:

$$g_\Box(t, \mathbf{x}) = \frac{\delta(t - R/c)}{4\pi R} \tag{9}$$

Here, $R = \|\mathbf{x}\|$, and because of the inherent symmetry in this problem it also makes sense to henceforth write $g_\Box = g_\Box(t, R)$.[1]

[1] The "box" symbol ($\Box$) represents the d'Alembert operator.

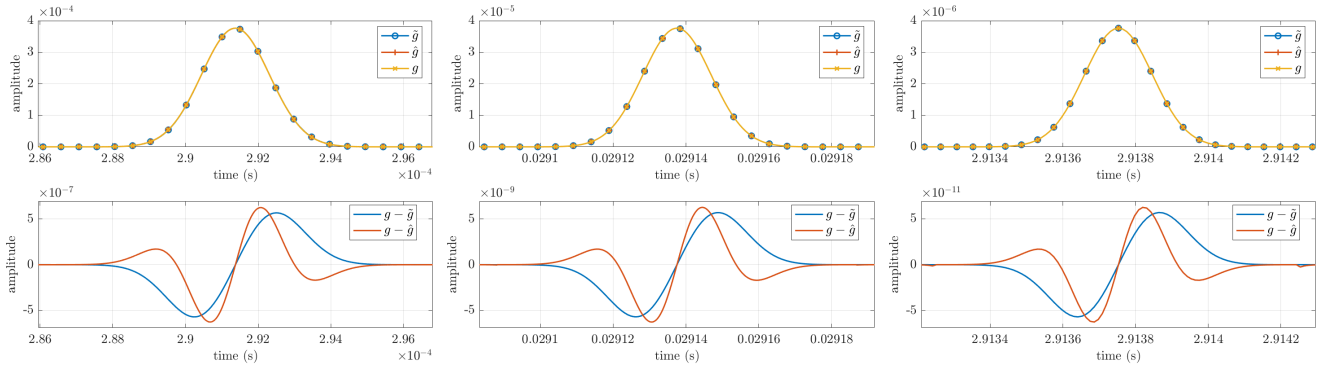

(a) $R = 0.1\,\text{m}$ (b) $R = 10\,\text{m}$ (c) $R = 1000\,\text{m}$

Figure 2: Evaluation of reference solution g and approximations $\tilde{g}$ and $\hat{g}$ for distances as indicated. Top: signals, bottom: errors

With $\gamma' > 0$ a closed-form expression for the Green's function g is currently not available. Fortunately, a close approximation is available in closed-form [30, 31, 32], which is useful for small γ' and large times t [32]. For this we can write $g \approx \tilde{g}$, where:

$$\tilde{g}(t, R) = \frac{u(t)}{4\pi R\sqrt{2\pi t\gamma'}} \exp\left(-\frac{(t - R/c)^2}{2t\gamma'}\right) \tag{10}$$

Here, $u(t)$ is the Heaviside function, which is included for causality. It is also useful to express this approximate Green's function as the following non-stationary convolution:

$$\tilde{g}(t, R) = g_{\square}(t, R) \otimes g_{\triangle}(t, t') = \int_{-\infty}^{\infty} g_{\square}(t - t', R) g_{\triangle}(t, t') dt' \tag{11}$$

where now:

$$g_{\triangle}(t, t') = \frac{u(t)}{\sqrt{2\pi t\gamma'}} \exp\left(-\frac{t'^2}{2t\gamma'}\right) \tag{12}$$

Thus, $\tilde{g}$ is equal to a convolution between the Green's function for the lossless wave equation and $g_{\triangle}$, a Gaussian smoothing kernel whose variance, $t\gamma'$, increases with time. In other words, $g_{\triangle}$ is responsible for the effect of a distance-dependent loss in high frequencies, where distance is simply linked to time through the speed of sound c. Similarly, it can be noted that $g_{\triangle}$ is itself the Green's function to a one-dimensional heat equation with t' representing a spatial coordinate [32].

3.2. Evaluation of approximation

While the accuracy of the approximation (10) has been evaluated in [32], this was done for viscosity and distance values in the context of soft tissues. In room acoustics, distances are longer and viscosity constants are smaller. A complete validation of this approximation in all air conditions and distances possible for room acoustics is outwith the scope of this paper, so only the conditions in Fig. 1 will be evaluated in this section for brevity, and the same methodology (coming from [32]) can be applied to other parameter combinations if so desired.

Considering then air conditions of 20°C and 50% relative humidity, with an associated sound speed of 343.2 m/s, we can calculate a reference solution using the inverse Fourier transform and the dispersion relation (6):

$$g(t, R) = \frac{\mathcal{F}^{-1}\left(e^{-\Im\{\hat{k}\}R} e^{-i\Re\{\hat{k}\}R}\right)}{4\pi R} \tag{13}$$

where $\hat{k} = \hat{k}(\omega)$ and the above is evaluated with regularly-spaced samples in time and frequency, and $\mathcal{F}^{-1}(\cdot)$ is carried out using an inverse DFT. Comparisons of g and $\tilde{g}$ (sampled in the time-domain) are shown in Fig. 2 for distances $R \in \{0.1, 10, 1000\}$ m. It can be seen that in these cases g and $\tilde{g}$ are indistinguishable ($\hat{g}$ will be defined and discussed shortly), and errors are small relative to signals. In these examples, signal-to-noise (SNR) ratios are -55dB, -74dB, and -94dB, respectively. It is important to note that while one can reasonably expect distances between source and receiver to be greater than 10 cm in room acoustics scenarios, errors will tend to increase as distances between source and receiver decrease (as expected). It is also worth mentioning that air absorption can be, and is generally, completely ignored over short distances.

3.3. Further approximations

There are two minor issues to deal with for practical use of this Gaussian kernel: a) it is infinite in extent and b) the "variance" is a function of time, so one cannot directly calculate a suitable truncation point (e.g., in terms of a dB drop relative to peak). While root-finding methods could be employed to find truncation points, it is straightforward apply a further simplification that avoids these extra steps. To this end, we expand (11) as:

$$\tilde{g}(t, R) = \int_{-\infty}^{\infty} \frac{\delta(t - t' - R/c)}{4\pi R} \frac{u(t)}{\sqrt{2\pi t\gamma'}} \exp\left(-\frac{t'^2}{2t\gamma'}\right) dt' \tag{14}$$

By the sifting property of the Dirac delta, the terms inside the integral are only contributing at local times $t = t' + R/c$, but since we expect $t' \ll R/c$ at those local times, we can also make the approximation $t \approx R/c$ where t appears in the denominator (leaving $u(t)$ intact). With this we arrive at the following approximation:

$$\hat{g}(t, R) = \frac{u(t)}{4\pi R\sqrt{2\pi t_R\gamma'}} \exp\left(-\frac{(t - t_R)^2}{2t_R\gamma'}\right) \tag{15}$$

where $t_R = R/c$. From another point of view, the variance $t\gamma'$ can be assumed to be constant over the short local time support of the

Gaussian, even for long times t (within reason for room acoustics) because $\gamma' \lll 1$. As we have replaced the time-varying variance, $t\gamma'$, with a constant variance $t_R\gamma'$, this allows for a simple evaluation of a truncation point for the smoothing kernel. For a relative truncation level of $-N_{\text{dB}}$ relative to its peak, one can then calculate:

$$\Delta_t = \sqrt{0.1\ln(10)N_{\text{dB}}t_R\gamma'} \tag{16}$$

and the kernel need only be evaluated in the range $[t_R-\Delta_t, t_R+\Delta_t]$.

This truncated approximation has also been evaluated for air conditions of 20°C and 50% relative humidity, which can be seen in Fig. 2 for distances $R \in \{0.1, 10, 1000\}$ m and with $N_{\text{dB}} = 120$. It can be seen that g and $\hat{g}$ are indistinguishable, and errors are small relative to signals, but truncation points become apparent in error signals after long times (and, as would be expected, sooner if N_{dB} is less). With this approximation, SNRs are -56 dB, -75 dB, and -95 dB, respectively. While $\hat{g}$ happens to give a slightly better approximation here than $\tilde{g}$, it is expected that as distances increase $\tilde{g}$ will be the more accurate approximation for a given N_{dB} as truncation errors become more significant.

4. USE IN ROOM ACOUSTICS SIMULATIONS

So far we have only considered a single impulsive sound event in free space. In the context of room acoustics, the sound arriving at a receiver is comprised of a multitude of arriving wavefronts, with additional frequency-dependent dissipation due to wall reflections. Within geometrical acoustics simulations, where wavefronts are taken to be carried by rays coming from virtual image sources, one can simply replace the usual lossless Green's function g applied to each ray or image source [8] with the dissipative $\hat{g}$, and wall reflections may be applied as usual.

Along these lines, a time-domain room impulse response $x(t)$ could be viewed as the following discrete sum of convolutions:

$$x(t) = \sum_i \int_{-\infty}^{\infty} h_i(\tau) g_{\square}(t-\tau, R_i) d\tau = \sum_i \frac{h_i(t-R_i/c)}{4\pi R_i} \tag{17}$$

where $h_i(t)$ is the filter response attributed to ith arriving wavefront – taking into account total contributions of frequency-dependent reflections or diffraction (e.g.) – and $g_{\square}$ is the Green's function of the lossless wave equation parametrised with the total distance R_i travelled by that wavefront through the room (starting from the source). The precise combination of filters h_i is not important and does not have to be unique for this point of view, but in the context of geometrical acoustics each filter would characterise the sound travelling along a ray coming from an image source (undergoing various wall reflections and/or diffractions).

In order to apply air absorption to $x(t)$, we replace $g_{\square}$ with $\tilde{g}$ to get a new signal $y(t)$:

$$y(t) = \sum_i \int_{-\infty}^{\infty} h_i(\tau) \int_{-\infty}^{\infty} \frac{\delta(t-\tau-R_i/c-t')}{4\pi R_i} g_{\triangle}(t,t') dt' d\tau \tag{18a}$$

$$= \int_{-\infty}^{\infty} \sum_i \frac{h_i(t-R_i/c-t')}{4\pi R_i} g_{\triangle}(t,t') dt' \tag{18b}$$

$$= \int_{-\infty}^{\infty} x(t-t') g_{\triangle}(t,t') dt' \tag{18c}$$

Thus, if it is possible to represent a room impulse response simulated without air absorption as (17), we can simply apply the diffusion kernel $g_{\triangle}$ through a time-varying convolution as shown above to add air absorption. We note that implicit here would be the assumption that air absorption has negligible effects at wall reflections (i.e., the filters $h_i(t)$ are unchanged in the presence of air absorption). However, this is a rather weak assumption since we know that air absorption will not cause significant relative changes over short time scales (e.g., the instant of a reflection).[2] Indeed, this is the same reasoning behind the use of $\hat{g}$ as an approximation for g, which showed a good agreement with g in free space.

To summarise, the methodology for using this air absorption filter in room acoustics simulations is as follows:

1. Simulate room acoustic impulse responses with wall absorption and lossless air.
2. Post-process each impulse response $x(t)$ with the time-varying convolution $y(t) = x(t) \otimes g_{\triangle}(t,t')$ to get an output impulse response $y(t)$ with air absorption applied.

In discrete form, and taking into account the truncated approximation $\hat{g}$, this convolution can be expressed as:

$$y[n] = \sum_{n'=-\lceil\Delta_n\rceil}^{\lceil\Delta_n\rceil} x[n-n'] \frac{u[n]}{\sqrt{2\pi n T_s \gamma'}} \exp\left(-\frac{(n'T_s)^2}{2nT_s\gamma'}\right) T_s \tag{19}$$

where $u[n]$ is the unit step and $\Delta_n = F_s\Delta_t$. Finally, it is suggested to set $y[n] = x[n]$ for $n < \frac{T_s}{2\pi\gamma'}$, during which time the diffusion kernel has an effective time support smaller than T_s. Since the sample index relates directly to a distance travelled, any "pre-delay" should be removed from $x[n]$ prior to filtering.

5. NUMERICAL EXPERIMENTS

Numerical experiments are conducted in this section to illustrate the use of the proposed air absorption filter in the context of geometrical acoustics simulations and wave-based simulations. Sound examples are provided at the accompanying website [33].

5.1. Image source simulation - simple shoebox room

We start with a simple simulation of a shoebox room using the traditional image-source method [34]. We consider a room with dimensions $7.0 \times 5.0 \times 2.8$, in metres, with a Sabine absorption coefficient of 0.03 on all walls. The source is at position $(6.1, 2.0, 1.5)$, in metres, and the receiver at $(3.2, 2.0, 1.5)$, in metres. The room is illustrated in Fig. 3. The speed of sound is set to $c = 343.2$ m/s and $\gamma' = 3.0$ ns, according to air conditions of 20°C and 50% relative humidity. The corresponding impulse response, calculated with 320 orders of image sources, has a spectrogram shown in Fig. 4, without air absorption (top) and with air absorption applied using the proposed method (middle).[3] Additionally, the Python package *pyroomacoustics* [13] is used to simulate the same scene with distance-based air attenuation applied to image sources and the result is shown in the bottom spectrogram in Fig. 4.[4]

The effect of applying the air absorption filter is clearly seen in comparing the first two spectrograms in Fig. 4. Additionally, one

[2] Entropy and vorticity modes and boundary-layers effects are also present [22], but these are typically neglected in the context of room acoustics (e.g., as in [25]).

[3] Spectrograms are computed with 1024-sample Hann-windowing and 75% frame overlap.

[4] Octave-band coefficients are derived from (2) and used in place of default attenuation parameters selected by *pyroomacoustics* for these air conditions. See [33] for supplementary results with default selected parameters.

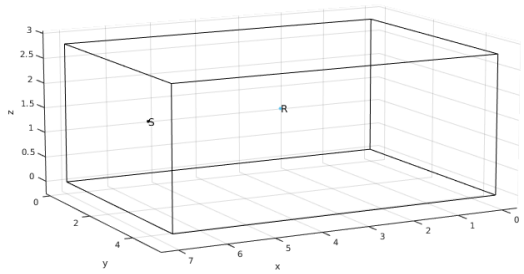

Figure 3: Shoebox room setup

can clearly see the "stairstep" effect of assuming one attenuation coefficient per octave band in the bottom spectrogram, with attenuation deviating from the expected power-law, especially in the upper two octave bands where air attenuation is most significant.

5.2. Wave-based simulation - simple shoebox room

Having shown how the filtering approach may be used with geometrical acoustics simulations, we also show it can be used with wave-based simulations, using a finite-difference time-domain (FDTD) method. The intention here is not to compare image-source outputs to FDTD outputs, but rather to compare FDTD outputs with and without air absorption, using the filter approach and using a viscothermal FDTD scheme (i.e., via direct simulation of Stokes' equation) [5, 7].

In this example we consider a normal-incidence absorption coefficient of 0.04 on all walls in the otherwise identical room setup. We use the simplest finite-difference time-domain (FDTD) simulation for the lossless wave equation [35], computed in double precision with a grid spacing chosen for 7.5 points per wavelength (PPW) at the wavelength corresponding to $f_{\max} = 11$ kHz, such that numerical dispersion error is less than two percent under $f_{\max}$ [36], which ultimately requires 24 GB of computer memory. The time-step is set to the Courant limit ($1/T_s \approx 294$ kHz), and the output impulse response is resampled to 48 kHz. The same room is also simulated with a viscothermal wave equation FDTD scheme (after [37]), which simulates $\tilde{\alpha}_{\mathrm{O}_2}(\omega)$ through Stokes' equation directly, for which 36GB of memory is required in this case (a 50% increase). Spectrograms of the resulting signals are shown in Fig. 5: without (top) and with (middle) the air absorption filter applied; and using the viscothermal scheme (bottom). It can be seen that the use of the air absorption filter reproduces the same behaviour as the viscothermal scheme, while using 33% less memory.[5]

It is also worth comparing the time-domain signals of the impulse responses which include air absorption. These are shown in Fig. 6, where y_1 is the result of the lossless FDTD scheme with the air absorption filter, and y_2 the result of the viscothermal scheme. It can be seen that there are indeed differences between the signals, as show in the bottom frame of Fig. 6. These discrepancies are due to the approximate nature of the filter, and to the fact that the air absorption component in the FDTD scheme suffers from numerical dissipation error (as analysed in [7]), while the air absorption filter does not. This can lead to small phase errors that can give rise to seemingly large time-domain residuals, but this does not imply that such errors are perceptible.[6]

[5] See [5, 7] for more on viscothermal FDTD simulation costs.

[6] Readers are invited to listen to audio examples at [33].

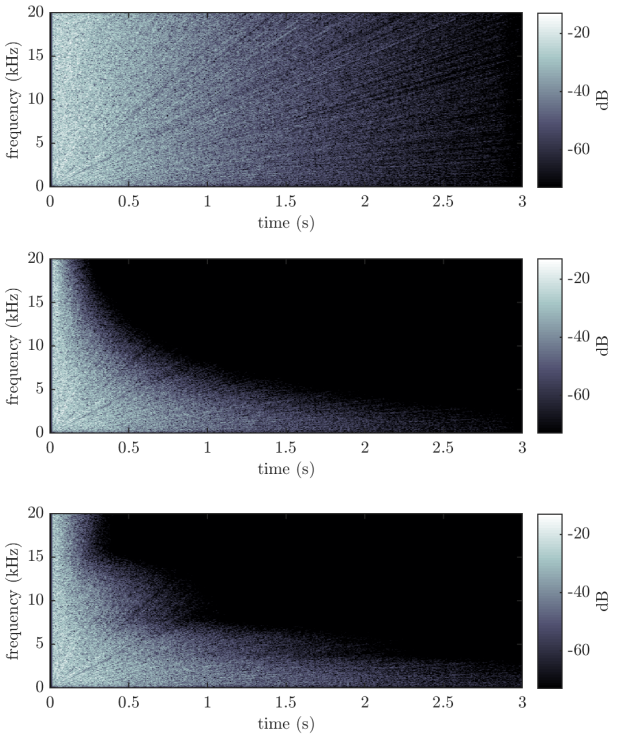

Figure 4: Room impulse response spectrograms. Top: image source method (ISM), without air absorption; middle: ISM + air absorption filtering; bottom: ISM computed with the Python package *pyroomacoustics* with air absorption [13].

For another point of comparison, we calculate the signals' similarities in the frequency domain using the following metric which measures geometric similarity between complex STFT frames:

$$\sigma_s(t) = \frac{\|Y_1(t,\omega)Y_2^*(t,\omega)\|_\omega}{\|Y_1(t,\omega)\|_\omega \|Y_2(t,\omega)\|_\omega} \tag{20}$$

Here $Y_1(t,\omega)$ and $Y_2(t,\omega)$ represent the STFTs of $y_1(t)$ and $y_2(t)$ (e.g., those shown in (6)), and the Euclidean norms are calculated across the frequency-dimension. This similarity metric – which is less susceptible to phase differences than taking time-domain residuals – returns a real value between zero and one as a function of time (STFT frame times). We plot $\log_{10}(1-\sigma_s)$ in Fig. 7, where we see that the STFT frames are generally more than 99% similar across the signals' durations. This indicates that the signal differences in Fig. 6 could be negligible. It is important to remember that phase errors as large as two milliseconds may not be audible (see, e.g., [38]).

5.3. Wave-based simulation - complex shoebox room

The previous example with wave-based simulations shows that the proposed method works with a simple shoebox room with frequency-independent impedance boundary conditions. However, that does not necessarily imply the technique works in a more complex room scene. To this end, we test a similarly-sized room with the same source and receiver positions, but now with diffusive irregularities introduced at one wall, as pictured in Fig. 10. Additionally, frequency-dependent, complex impedance boundary conditions are used in place of frequency-independent ones, following the viscothermal

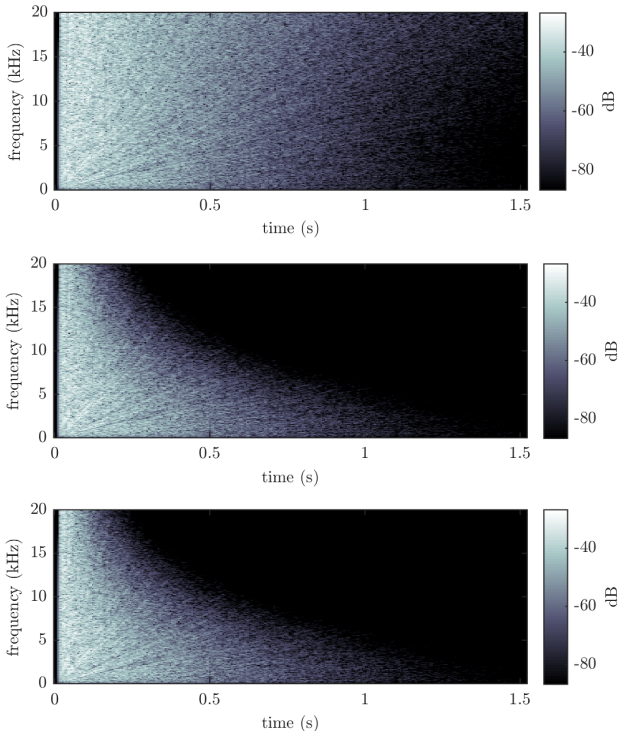

Figure 5: Room impulse response spectrograms. Top: lossless FDTD (without air absorption); middle: lossless FDTD + air absorption filtering; bottom: viscothermal FDTD.

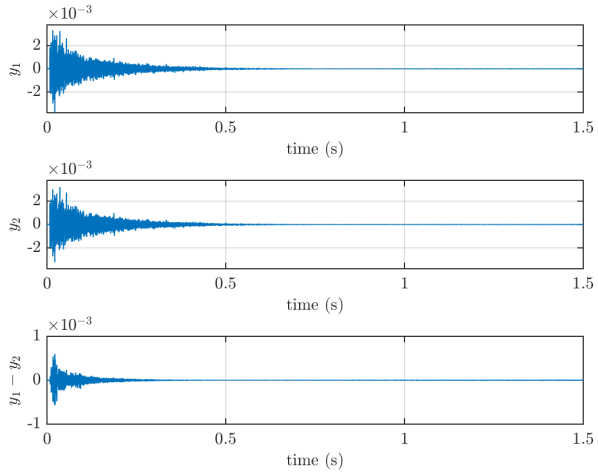

Figure 6: Room impulse responses simulated using FDTD methods: y_1 the lossless scheme + air absorption filter; y_2 the viscothermal scheme.

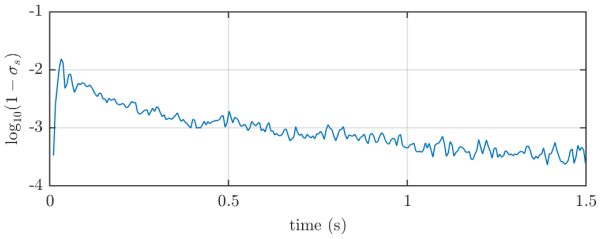

Figure 7: Room impulse response differences (one minus similarity between zero and one), computed using STFT frame similarity (20).

FDTD scheme detailed in [37]. Passive impedances [25] are chosen such that per-octave-band Sabine absorption coefficients vary in the range 0.02–0.04. The diffusing elements introduce diffraction/scattering into the room response, which tests the methodology laid out the previous section. Using the same analyses as before, results are shown in Figs. 8 and 9. Fig. 8 shows the spectrograms of results from the lossless wave equation without (top) and with the air absorption filter (middle), and that from the viscothermal scheme (bottom). In this case temporal signals including air absorption are not shown for brevity, but their spectral similarities are shown in Fig. 9.

As expected, these figures show that the use of the filter returns similar decay behaviour to that from the viscothermal scheme. Thus, despite the added effects of diffraction and frequency-dependent wall impedances, the air absorption filtering approach shows good agreement to the viscothermal FDTD output, with STFTs again showing, generally, similarities of at least 99%.

It is worth pointing out that in the preceding examples, the perfect symmetry of a rectangular room gave rise to sweeping echoes, which are visible in Figs. 4 and 5 as slight diagonal lines representing linear chirps, as predicted by theory [39]. In this case, the effect of diffusing/scattering elements prevents sweeping echoes from appearing (see Fig. 8).

6. CONCLUSIONS AND FINAL REMARKS

In this paper, a method for including air absorption in room acoustics simulations was presented, which is based on an approximate Green's function solution to Stokes' equation. This approximate Green's function was parametrised to reproduce the oxygen relaxation effect in air absorption, which is the dominant effect for common indoor conditions. A further truncated and symmetric approximation was provided, and a discrete implementation was laid out. Numerical experiments were conducted to demonstrate the utility of this approach in both geometrical and wave-based simulations, with accompanying sound examples available at [33].

The proposed filtering approach is advantageous for wave-based FDTD simulations because it leads to at least a 33% decrease in memory usage over viscothermal FDTD schemes [7], thereby bringing down costs of simulation-based case studies (e.g., [40]). Additionally, numerical dissipation error can be avoided [7]. In the context of geometrical acoustics simulations, this method could be a preferable alternative to existing approaches, as it avoids the need for filter fitting, and the entire approach is parametrised by a few physical parameters (and a truncation level N_{dB}).

An important limitation of the proposed method is that it applies only to impulse response simulations, which, by definition, includes static monopole point sources and receivers. Since only the distances travelled by sound waves matter for air attenuation and not directions of propagation (air absorption is isotropic), this approach could also be used with directional point-sources [41], directional point-receivers [42], and in the far field of distributed sources [43].

Another limitation of this method is the suitability of power-law air attenuation to a chosen set of air conditions. If variations from power-law attenuation due to the relaxation effects need to be

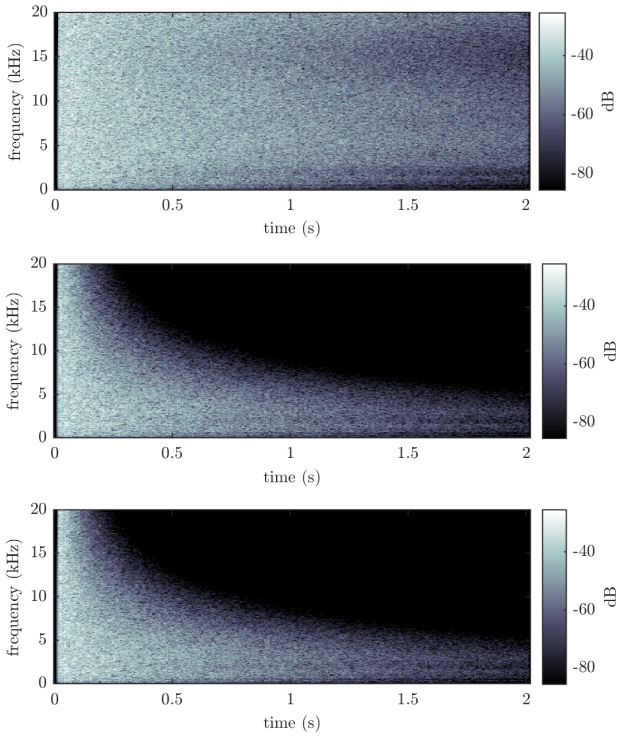

Figure 8: Room impulse response spectrograms. Top: lossless FDTD (without air absorption); middle: lossless FDTD + air absorption filtering; bottom: viscothermal FDTD.

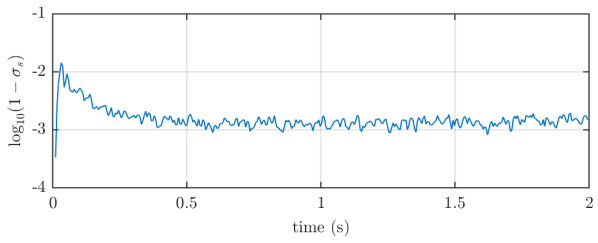

Figure 9: Room impulse responses differences (one minus similarity between zero and one), computed using STFT frame similarity (20).

modelled, this approach may not be appropriate. For such cases, options include using filter-based approaches to post-process room impulse responses (e.g., applying attenuation via short-time Fourier transform [18]), or developing wave-based room acoustic models with full air absorption effects (e.g. building on [44]).

7. REFERENCES

[1] L. Savioja and N. Xiang, "Simulation-based auralization of room acoustics," *Acoustics Today*, vol. 16, no. 4, pp. 48–55, 2020.

[2] V. Välimäki, J. D. Parker, L. Savioja, J. O. Smith III, and J. S. Abel, "Fifty years of artificial reverberation," *IEEE Trans. Audio, Speech, Lang. Process.*, vol. 20, no. 5, pp. 1421–1448, 2012.

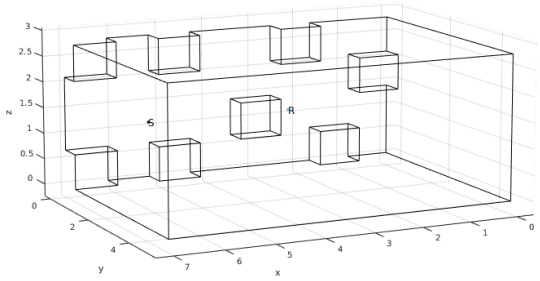

Figure 10: Diffusive room setup

[3] D. Fogerty, A. Alghamdi, and W.-Y. Chan, "The effect of simulated room acoustic parameters on the intelligibility and perceived reverberation of monosyllabic words and sentences," *J. Acoust. Soc. Am.*, vol. 147, no. 5, pp. EL396–EL402, 2020.

[4] M. S. Wochner, A. A. Atchley, and V. W. Sparrow, "Numerical simulation of finite amplitude wave propagation in air using a realistic atmospheric absorption model," *J. Acoust. Soc. Am.*, vol. 118, no. 5, pp. 2891–2898, 2005.

[5] C. J. Webb and S. Bilbao, "Computing room acoustics with CUDA - 3D FDTD schemes with boundary losses and viscosity," in *Proc. IEEE Int. Conf. Acoust., Speech, Signal Process.*, Prague, Czech Republic, 2011, pp. 317–320.

[6] J. Botts and L. Savioja, "Extension of a spectral time-stepping domain decomposition method for dispersive and dissipative wave propagation," *J. Acoust. Soc. Am.*, vol. 137, no. 4, pp. EL267–EL273, 2015.

[7] B. Hamilton, S. Bilbao, and C. J. Webb, "Improved finite difference schemes for a 3-D viscothermal wave equation on a GPU," in *Proc. Forum Acusticum*, Krakow, Poland, Sept. 2014.

[8] M. Vorländer, *Auralization: Fundamentals of Acoustics, Modelling, Simulation, Algorithms and Acoustic Virtual Reality*, Springer, 2nd edition, 2020.

[9] J. A. Moorer, "About this reverberation business," *Comp. Music J.*, pp. 13–28, 1979.

[10] J.-M. Jot and A. Chaigne, "Digital delay networks for designing artificial reverberators," in *AES Convention 90*. Audio Engineering Society, 1991.

[11] J.-M. Jot, "Proportional parametric equalizers—Application to digital reverberation and environmental audio processing," in *AES Convention 139*. Audio Engineering Society, 2015.

[12] D. Schröder, *Physically based real-time auralization of interactive virtual environments*, vol. 11, Logos Verlag Berlin GmbH, 2011.

[13] R. Scheibler, E. Bezzam, and I. Dokmanić, "Pyroomacoustics: A Python package for audio room simulation and array processing algorithms," in *Proc. IEEE Int. Conf. Acoust., Speech, Signal Process.*, 2018, pp. 351–355.

[14] J. Huopaniemi, L. Savioja, and M. Karjalainen, "Modeling of reflections and air absorption in acoustical spaces a digital filter design approach," in *Proc. IEEE Worksh. Appl. Signal Process. Audio & Acoust.*, 1997, pp. 4–pp.

[15] L. Savioja, T. Huopaniemi, J.and Lokki, and R. Väänñen, "Creating interactive virtual acoustic environments," *J. Audio Eng. Soc.*, vol. 47, no. 9, pp. 675–705, Sept. 1999.

[16] J. M. Kates and E. J. Brandewie, "Adding air absorption to simulated room acoustic models," *J. Acoust. Soc. Am.*, vol. 148, no. 5, pp. EL408–EL413, 2020.

[17] A. Southern, S. Siltanen, D. Murphy, and L. Savioja, "Room impulse response synthesis and validation using a hybrid acoustic model," *IEEE Trans. Audio, Speech, Lang. Process.*, vol. 21, no. 9, Sept. 2013.

[18] J. Saarelma, J. Califa, and R. Mehra, "Challenges of distributed real-time finite-difference time-domain room acoustic simulation for auralization," in *AES Int. Conf. Spatial Reproduction*, July 2018.

[19] D. Griffin and J. Lim, "Signal estimation from modified short-time fourier transform," *IEEE Trans. Audio, Speech, Signal Process.*, vol. 32, no. 2, pp. 236–243, 1984.

[20] L. Savioja, "An open-access interactive textbook for teaching room acoustics modeling," *J. Acoust. Soc. Am.*, vol. 139, no. 4, pp. 2033–2033, 2016.

[21] J. Saarelma and L. Savioja, "Audibility of dispersion error in room acoustic finite-difference time-domain simulation in the presence of absorption of air," *J. Acoust. Soc. Am.*, vol. 140, no. 6, pp. EL545–EL550, 2016.

[22] A. D. Pierce, *Acoustics*, chapter Effects of Viscosity and Other Dissipative Processes, Springer, 2019.

[23] "Acoustics – Attenuation of sound during propagation outdoors. Part 1: Calculation of the absorption of sound by the atmosphere," Standard ISO 9613–1, International Organization for Standardization, Geneva, Switzerland, 1993.

[24] H. E. Bass, L. C. Sutherland, A. J. Zuckerwar, D. T. Blackstock, and D. M. Hester, "Atmospheric absorption of sound: Further developments," *J. Acoust. Soc. Am.*, vol. 97, no. 1, pp. 680–683, 1995.

[25] S. Bilbao and B. Hamilton, "Wave-based room acoustics simulation: Explicit/implicit finite volume modeling of viscothermal losses and frequency-dependent boundaries," *J. Audio Eng. Soc.*, vol. 65, no. 1/2, pp. 78–89, 2017.

[26] R. H. C. Wenmaekers, C. C. J. M. Hak, and M. C. J. Hornikx, "The effective air absorption coefficient for predicting reverberation time in full octave bands," *J. Acoust. Soc. Am.*, vol. 136, no. 6, pp. 3063–3071, 2014.

[27] E. Zwicker and H. Fastl, *Psychoacoustics: Facts and models*, Springer Science & Business Media, 3rd edition, 2007.

[28] G. G. Stokes, "Sound attenuation due to viscosity," *Trans. Cambridge Phil. Soc.*, vol. 8, pp. 75–102, 1845.

[29] G. Barton, *Elements of Green's Functions and Propagation: Potentials, Diffusion, and Waves*, Oxford University Press, 1989.

[30] D. G. Crighton, A. P. Dowling, J. E. Ffowcs-Williams, M. Heckl, F. G. Leppington, and J. F. Bartram, "Modern methods in analytical acoustics lecture notes," 1992.

[31] M. J. Buckingham, "Causality, Stokes' wave equation, and acoustic pulse propagation in a viscous fluid," *Phys. Rev. E*, vol. 72, no. 2, pp. 026610, 2005.

[32] J. F. Kelly and R. J. McGough, "Causal impulse response for circular sources in viscous media," *J. Acoust. Soc. Am.*, vol. 123, no. 4, pp. 2107–2116, 2008.

[33] B. Hamilton, "DAFx2021: Accompanying sound examples," `https://brianhamilton.co/DAFx20in21/`, 2021-05-24.

[34] J. B. Allen and D. A. Berkley, "Image method for efficiently simulating small-room acoustics," *J. Acoust. Soc. Am.*, vol. 65, pp. 943, 1979.

[35] L. Savioja, T. J. Rinne, and T. Takala, "Simulation of room acoustics with a 3-D finite difference mesh," in *Proc. Int. Comp. Music Conf.*, Danish Institute of Electroacoustic Music, Denmark, 1994, pp. 463–466.

[36] B. Hamilton, *Finite Difference and Finite Volume Methods for Wave-based Modelling of Room Acoustics*, Ph.D. thesis, University of Edinburgh, 2016.

[37] B. Hamilton, C. J. Webb, N. D. Fletcher, and S. Bilbao, "Finite difference room acoustics simulation with general impedance boundaries and viscothermal losses in air: Parallel implementation on multiple GPUs," in *Proc. Int. Symp. Music & Room Acoust.*, Buenos Aires, Argentina, Sept. 2016.

[38] J. Saarelma, J. Botts, B. Hamilton, and L. Savioja, "Audibility of dispersion error in room acoustic finite-difference time-domain simulation as a function of simulation distance," *J. Acoust. Soc. Am.*, vol. 139, no. 4, pp. 1822–1832, 2016.

[39] E. De Sena, N. Antonello, M. Moonen, and T. van Waterschoot, "On the modeling of rectangular geometries in room acoustic simulations," *IEEE/ACM Trans. Audio, Speech, Lang. Process.*, vol. 23, no. 4, pp. 774–786, 2015.

[40] H. Lai and B. Hamilton, "Computer modeling of barrel-vaulted sanctuary exhibiting flutter echo with comparison to measurements," *Acoustics*, vol. 2, no. 1, pp. 87–109, 2020.

[41] S. Bilbao and B. Hamilton, "Directional sources in wave-based acoustic simulation," *IEEE/ACM Trans. Audio, Speech, Lang. Process.*, vol. 27, no. 2, pp. 415–428, 2018.

[42] S. Bilbao, A. Politis, and B. Hamilton, "Local time-domain spherical harmonic spatial encoding for wave-based acoustic simulation," *IEEE Signal Process. Lett.*, vol. 26, no. 4, pp. 617–621, 2019.

[43] S. Bilbao and J. Ahrens, "Modeling continuous source distributions in wave-based virtual acoustics," *J. Acoust. Soc. Am.*, vol. 148, no. 6, pp. 3951–3962, 2020.

[44] B. Hamilton and S. Bilbao, "FDTD modelling of sound propagation in air including viscothermal and relaxation effects," in *Proc. e-Forum Acusticum*, Lyon, France, Dec. 2020.